Europe PMC Funders Group
Author Manuscript
Cancer Res. Author manuscript; available in PMC 2013 January 01.

Published in final edited form as:
Cancer Res. 2012 July 1; 72(13): 3424–3436. doi:10.1158/0008-5472.CAN-12-0423.

FRMD4A upregulation in human squamous cell carcinoma promotes tumor growth and metastasis and is associated with poor prognosis

Stephen J. Goldie[1], **Klaas W. Mulder**[1], **David Wei-Min Tan**[2], **Scott K. Lyons**[1], **Andrew H. Sims**[3], and **Fiona M. Watt**[1,2]

[1]CRUK Cambridge Research Institute, Li Ka Shing Centre, Robinson Way, Cambridge CB2 0RE

[2]Wellcome Trust Centre for Stem Cell Research, Tennis Court Road, Cambridge CB2 1QR

[3]Breakthrough Research Unit, MRC IGMM, University of Edinburgh, Carrington Crescent, Edinburgh, EH4 2XR

Abstract

New therapeutic strategies are needed to improve treatment for head and neck squamous cell carcinoma (HNSCC), an aggressive tumor with poor survival rates. FRMD4A is a human epidermal stem cell marker implicated previously in epithelial polarity that is upregulated in SCC cells. Here we report that FRMD4A upregulation occurs in primary human HNSCC where high expression levels correlate with increased risks of relapse. FRMD4A silencing decreased growth and metastasis of human SCC xenografts in skin and tongue, reduced SCC proliferation and intercellular adhesion, and stimulated caspase-3 activity and expression of terminal differentiation markers. Notably, FRMD4A attenuation caused nuclear accumulation of YAP, suggesting a potential role for FRMD4A in Hippo signaling. Treatment with the HSP90 inhibitor 17-DMAG or ligation of CD44 with hyaluronan caused nuclear depletion of FRMD4A, nuclear accumulation of YAP and reduced SCC growth and metastasis. Together, our findings suggest FRMD4A as a novel candidate therapeutic target in HNSCC based on the key role in metastatic growth we have identified.

Keywords

squamous cell carcinoma; FERM domain containing protein; xenografts; Hippo pathway; CD44

Introduction

Squamous cell carcinoma (SCC) of the skin and oral cavity pose differing threats to health. Skin SCCs are very common and rarely metastasise; they can often be cured by surgery alone (1). SCCs in the oral cavity (head and neck SCC; HNSCC) are less common, but tend to present at an advanced stage (2). Despite radical surgery and adjuvant therapy, HNSCC lesions often recur and spread to other body sites. Survival rates for oral SCC are approximately 50% and have not improved for 30 years.

Both skin SCC and HNSCC arise from multi-layered epithelia, which are maintained by stem cells residing in the basal epithelial layer, attached to an underlying basement

Corresponding author: Fiona.watt@cancer.org.uk; telephone: +44 1223 760246; fax: +44 1223 760287.

Conflicts of interest: none

Europe PMC Funders Author Manuscripts
Europe PMC Funders Author Manuscripts

Europe PMC Funders Author Manuscripts

Europe PMC Funders Author Manuscripts

membrane (3). Skin SCC and HNSCC exhibit cellular heterogeneity, with some cells expressing markers of the normal terminal differentiation process while others are undifferentiated. There is also good evidence for functional heterogeneity, both in terms of clonal growth of SCC cells in vitro (4, 5) and in xenografts in immune compromised mice (6). Thus, SCC is one of the tumour types for which there is experimental support for the existence of cancer stem cells (tumour initiating cells) (7).

Using single cell gene expression profiling, we identified FERM domain containing 4A (FRMD4A) mRNA as a marker of cultured human epidermal stem cells (8). When we examined expression of a panel of 14 epidermal stem cell markers in cultured HNSCC cells, FRMD4A was the only marker that was consistently highly upregulated in HNSCC and thus emerged as a candidate HNSCC stem cell marker (5). FRMD4A was recently reported to connect the Par-3 complex to Arf6 guanine-nucleotide exchange factor and regulate assembly of adherens junctions in cultured mammary epithelial cells (9).

We have now characterised FRMD4A expression and function in SCC and present evidence that it is an attractive target for novel therapies to control SCC growth and metastasis.

Materials and Methods

Analysis of FRMD4A levels in published datasets

Processed gene expression data from two published HNSCC studies (10, 11) were downloaded from NCBI GEO (Accession numbers GSE10300 and GSE686). The X-Tile program (12) was used to determine the optimal cut-point for Kaplan Meier analysis performed using the ‘survival’ package for R, while correcting for the use of minimum P statistics.

Human tissue specimens

Work with human material was carried out in compliance with the UK Human Tissue Act (2004) and approved by the National Research Ethics Service (08/H0306/30). Appropriate informed consent was obtained from patients diagnosed with oral SCC, prior to operation at Addenbrooke’s Hospital. Small biopsy specimens were removed from freshly resected oral SCCs. Specimens of normal skin were obtained with informed consent from operations to remove excess skin.

For laser capture microdissection, tissue was frozen in OCT and sectioned with a cryostat. Sections were briefly air-dried and stained with cresyl violet. Using the Zeiss/P.A.L.M. Laser Capture Microdissection system the basal and granular epidermal layers were collected separately from two serial sections and material from both sections was pooled. RNA was isolated using RNeasy (Quiagen), then reverse transcribed with an Superscript III kit (Invitrogen).

Cell culture and lentiviral transduction

SCC13 and SCC25 (13) and keratinocytes from normal human epidermis (ky passage 4) and oral mucosa (CRI-005 passage 4) were cultured as described previously (5, 8), except that SCC lines were grown without a feeder layer of J2 3T3 cells. SCC13 and SCC25 cells were passaged for less than 6 months following thawing. SCC25 are available from ATCC (Manassas, Virginia) and validated by short tandem repeat profiling. The culture medium comprised FAD (three parts DMEM medium, one part Ham’s F12 medium, 1.8×10^{-4}M adenine) supplemented with 10% FCS, 0.5μg/ml hydrocortisone, 5μg/ml insulin, 10^{-10}M cholera toxin and 10ng/ml epidermal growth factor. SJG15 cells were derived from a SCC (pathological stage T2N1M0; well differentiated) on the lateral tongue of a 51-year old

Europe PMC Funders Author Manuscripts

Europe PMC Funders Author Manuscripts

female patient. Cells from the tumour were disaggregated in 0.25% trypsin/EDTA (Gibco) at 37°C then passaged on feeders until they became feeder-independent.

The YFP/Luciferase lentivirus construct was generated in-house. shRNA constructs were purchased from Open Biosystems. Viruses were packaged by transient transfection of 293T cells (14, 15). Viral supernatant was used to infect SCC cells. Infected cells were selected in hygromycin (YFP/Luciferase) or puromycin (shRNAs).

To stimulate keratinocyte differentiation, cells were grown in Keratinocyte Serum Free Medium (KSFM, Gibco) supplemented with 30 μg/ml Bovine Pituitary Extract and 0.2 ng/ml EGF for 2-3 days. Cells were then incubated in medium containing 10 μM AG1478 (Calbiochem) and/or 200 ng/ml recombinant human BMP2/7 heterodimer (R&D systems) for 48h.

For colony forming assays, 100 cells were plated in triplicate in 10cm plates without feeders. After 14 days, cultures were fixed and stained with 1% Rhodamine B and 1% Nile blue (Acros Organic). Colony-forming efficiency was calculated as the percentage of plated cells that formed a colony of three or more cells.

For real time imaging, 1000 cells were plated, in triplicate for each condition, in a 48-well plate without feeders and recorded using an Incucyte. Wells were imaged every 3 hours for 7 days.

Matrigel invasion assays were carried out using Boyden chambers (BD BioCoat™ Matrigel™ Invasion Chambers) in 24-well plates. Cells transduced with YFP/luciferase were serum starved in KSFM for 24 hours. 10^5 cells in KFSM were added per chamber in wells containing complete FAD medium. After 24 hours the Matrigel was removed from the well, and luciferin was added to the medium. The chambers were scanned and quantified using the IVIS.

For sphere forming assays, a 12-well plate was coated with polyHEMA to prevent adhesion of cells to the plastic. 100 cells were plated in methylcellulose in each well, in triplicate. After 21 days the wells were scanned and quantified using a Typhoon scanner.

Q-PCR

RNA was isolated and amplified as described previously (8). Q-PCR was performed using Taqman Gene Expression Assays for FRMD4A and transglutaminase (Applied Biosystems). All data were normalised to 18S.

Antibodies

SGO-3 and SGO-4 antibodies were raised by injecting FRMD4A peptide PPPQSLEGLRQMHYHRNDYDKC into rabbits. The antibodies were affinity purified on AminoLink® Plus Coupling Resin columns (Thermo scientific). The following antibodies were also used: α6 integrin (GoH3; BD Pharmigen, Oxford, UK), E-cadherin (HECD-1) (prepared in-house), GFP (Abcam, Cambridge, UK), Ki67 (Dako, UK), cleaved caspase-3 (R&D Systems, UK), YAP1 (Abcam), LATS1 (Abcam), MST1 (Abcam), Involucrin (SY3; prepared in-house), CD44 (BD Pharmigen, Oxford, UK), and GAPDH (Invitrogen). AlexaFluor-488 or -555 conjugated secondary antibodies and HRP conjugated secondary antibodies were purchased from Invitrogen.

Histology and in situ hybridisation

Tissue was either fixed in 10% neutral-buffered formalin and embedded in paraffin, or frozen in OCT embedding matrix (Raymond A. Lamb, UK). Epitope retrieval was

Europe PMC Funders Author Manuscripts

Europe PMC Funders Author Manuscripts

performed on paraffin sections by boiling in citrate buffer for 10 minutes. Blocking buffer contained 10% fetal calf serum, 4% bovine serum, 2.5% fish skin gelatin and 0.05% Tween 20. Staining was performed essentially as described previously (16). Immunofluorescence staining was imaged using a Leica Tandem Confocal microscope. Ki67 stained sections were photographed and analyzed using an Ariol SL-50 system (Applied Imaging, Corp.), as described previously (16). In situ hybridization was performed on sections of paraffin-fixed human foreskin, essentially as described previously (17).

Western blotting

Cells were disaggregated using trypsin/EDTA and collected by centrifugation. Cell pellets were lysed in RIPA buffer containing protease and phosphatase inhibitors (16) and subjected to polyacrylamide gel electrophoresis on 4% to 12% gradient gels. Proteins were transferred to nitrocellulose membranes and blocked in Tris buffer pH 8.0 containing 2.5% skimmed milk powder and 0.05% Tween 20. Blots were incubated with primary and secondary antibodies and visualised by enhanced chemiluminescence (16). Antibodies to FRMD4A and YAP were used at 1:200 dilution; anti-GAPDH was diluted 1:1000.

Xenografts

Experiments were subject to Cancer Research UK ethical review and performed under the terms of a U.K. Government Home Office license. NOD.Cg-*Prkdc*^{scid} *Il2rg*^{tm1Wjl}/SzJ (NSG) mice were purchased from the Jackson Laboratories (Maine, USA) and bred in-house. Mice were subject to inhalation anaesthesia during SCC implantation and IVIS imaging.

SCC cells were introduced into the anterior dorsal mucosa of the tongue with a 30g needle and 1ml syringe. For tail vein injections 2.5×10^5 cells in 50μl culture medium were introduced per mouse. To form tumours in back skin, silicone chambers were first implanted into a full thickness wound, as described previously (18). SCC cells were injected into the chamber and one week later the top of the chamber was cut off. After a further week the whole silicone chamber was removed.

Tumour size was determined by scanning mice in an IVIS 200 series imaging system (Caliper LifeSciences) following intraperitoneal injection of 15mg/ml D-Luciferin (potassium salt) dissolved in PBS (10μl/g). Tumour size was recorded weekly. To induce FRMD4A knockdown with doxycycline, mice were fed chow containing the drug (IPS Product Supplies UK).

To evaluate the effect of HA treatment, 10^6 SCC13 cells were implanted into the back skin. One week later tumour size was measured using the Xenogen IVIS and then each tumour was injected with 200μl of 0.1% HA (Sigma) or 200μl PBS alone.

To evaluate the effect of 17-DMAG treatment, 10^5 SCC25 cells were injected into the tongue. One week later tumour size was measured using the Xenogen IVIS and then each mouse received an intraperitoneal injection of 17-DMAG or vehicle control. Mice were subsequently injected once a week. For the first five weeks mice received 0.02mg 17-DMAG (Tocris). Thereafter the weekly dose was 0.04mg. A stock solution of 17-DMAG was prepared in 100% ethanol and diluted in PBS prior to injection. Control mice received injections of PBS alone.

Europe PMC Funders Author Manuscripts

Europe PMC Funders Author Manuscripts

Results

FRMD4A is expressed in the basal layer of human epidermis and is upregulated in HNSCC

To determine where FRMD4A (genome accession number NM_018027) is expressed in normal human epidermis we performed in situ hybridisation with a ^{35}S labelled probe to exon 25 (Figure 1A). FRMD4A transcripts were detected throughout the basal layer, where the stem cells reside (3, 8), but there was no signal above background in the suprabasal, differentiating cell layers. Hybridisation with a βa-actin probe provided a positive control as β-actin is expressed in all epidermal cell layers (Figure 1A).

Our observations were confirmed by q-PCR of mRNA isolated from the basal and upper differentiated (granular) layers of human epidermis following laser capture microdissection. The differentiation marker transglutaminase 1 was highly expressed in the granular layer and absent from the basal layer, whereas FRMD4A was upregulated in the basal layer and undetectable in the granular layer (Figure 1B). An inverse correlation between levels of FRMD4A and transglutaminase 1 was also observed in cultured human keratinocytes: addition of BMP2/7 and/or the EGF receptor antagonist AG1478 stimulated transglutaminase 1 expression and led to a corresponding decrease in FRMD4A (Figure 1B). We conclude that, as predicted for an epidermal stem cell marker (8), FRMD4A mRNA is expressed in basal layer keratinocytes and downregulated during terminal differentiation.

In addition to the FERM domain, FRMD4A is predicted (by motif scan analysis; 19) to have a coiled-coil domain, a bipartite nuclear localisation signal (NLS), a serine-rich C-terminal domain and numerous potential serine, threonine and tyrosine phosphorylation sites (Figure 1C and data not shown). In order to detect FRMD4A protein we raised rabbit antisera (SGO-3, 4) to a peptide that lies between the NLS and the serine-rich domain (Figure 1C). Both antibodies recognised a single band of approximately 76kD in Western blots of cultured human keratinocytes and SCC cells (SCC13, derived from a facial epidermal SCC; 13), somewhat smaller than the predicted size of 115 kDa (Figure 1C and data not shown). To evaluate antibody specificity, SCC13 cells were transduced with 5 different lentiviral shRNAs to FRMD4A or a scrambled shRNA control (SCR) (Figure 1C). All but one of the shRNAs (A9) caused a marked reduction in the abundance of the protein band detected by SGO-3 and SGO-4 (Figure 1C). As predicted from FRMD4A mRNA levels (5), the level of FRMD4A protein was higher in SCC13 than in primary keratinocytes cultured from epidermis (EK) or oral cavity (OK) (Figure 1C).

SGO-3 and SGO-4 were used to examine FRMD4A protein expression in sections of normal human skin and HNSCC. As predicted from the in situ hybridisation and q-PCR data, FRMD4A was expressed in the epidermal basal layer and downregulated in the suprabasal layers (Figure 1C). We next stained 13 tumours of the alveolar ridge, tongue and floor of mouth (6 well differentiated; 4 moderately differentiated; 3 poorly differentiated). FRMD4A protein was expressed throughout the epithelial compartment of human HNSCC and was upregulated regardless of pathological grade (Figure 1C).

To further evaluate the significance of FRMD4A upregulation in HNSCC, we examined published gene expression data from two collections of tumours (10, 11) using the X-Tile program (12). Kaplan Meier plots from both datasets showed a highly significant correlation between high levels of FRMD4A and risk of relapse (Figure 1D).

We conclude that in normal epidermis FRMD4A expression is confined to the basal layer, where the stem cells reside; that FRMD4A is widely expressed throughout the tumour mass in HNSCC; and that high FRMD4A levels are correlated with poor prognosis in HNSCC.

Europe PMC Funders Author Manuscripts

Europe PMC Funders Author Manuscripts

FRMD4A knockdown reduces cell-cell adhesion, growth and invasion in culture

We used SCC13 cells and a second human SCC line, SCC25 (derived from a tongue SCC; 13), to examine the consequences of reduced FRMD4A expression on SCC cell behaviour in vitro. In untransduced SCC13 (SCC13-WT) and SCC13 transduced with a scrambled shRNA control (SCC13-SCR) FRMD4A was located predominantly in the cytoplasm, with some localisation to the nucleus and partial colocalisation with E-cadherin at cell-cell borders (Figure 2A). FRMD4A knockdown (SCC13-A7) led to loss of FRMD4A in all locations and to a marked reduction in E-cadherin staining, which coincided with reduced cell-cell contact and elongated cell morphology (Figure 2A). Live cell imaging confirmed that whereas SCC13-WT and SCC13-SCR cells formed colonies with stable intercellular adhesions, SCC13-A7 cells did not (Supplemental Figure 1).

FRMD4A knockdown in SCC13 and SCC25 using several different shRNAs resulted in a reduction in colony forming efficiency, a surrogate readout of stem cell abundance (5) (Figure 2B). The reduction in colony formation correlated with an overall reduction in growth rate, as evaluated by live cell imaging (Supplemental Figure 1; Figure 2C). In addition, FRMD4A knockdown led to reduced SCC invasiveness in Boyden chamber assays and inhibition of anchorage dependent growth, as determined by sphere formation in suspension (Figure 2D).

Generation of an orthotopic xenograft model of human HNSCC

In HNSCC, death is frequently due to organ failure as a result of distant metastasis, rather than growth of the primary tumour (2). However, HNSCC growth in xenograft models is generally evaluated by the size of the primary tumour generated by grafting cells in a heterotopic site, the dorsal skin (6). To generate an improved xenograft model we transduced cultured SCC cells with a lentiviral construct that expressed a YFP/luciferase fusion protein so that tumour growth could be evaluated both macroscopically and microscopically (Figure 3A). Cells were either injected into a silicone chamber surgically implanted in the back skin (18) or directly injected into the tongue of NSG mice (Figure 3B). Primary tumours were evaluated in live mice using an IVIS 200 series imaging system (Caliper LifeSciences) following intraperitoneal injection of luciferin (Figure 3B). Organs were scanned post-mortem with an IVIS to detect metastatic disease (Figure 3B).

The tumorigenicity of SCCs depended on the location of the graft: chamber grafted SCCs required a minimum of 10^4 cells in order to successfully form a tumour in 100% of mice, whereas tongue grafted tumours developed after injection of only 100 cells (based on cohorts of 5 mice per group). The average survival times for mice injected with 10^4 SCC13 in the dorsal skin (73d) or 100 SCC13 cells (70d) in the tongue were similar, although the maximum survival time was greater in the tongue (135d versus 76d). In contrast, both the average (90d versus 61d) and maximum survival times (157d versus 73d) of SCC25 were greater in skin than in tongue. Thus each SCC line was more malignant when grafted into the location from which it was derived.

Histological analysis of skin xenografts revealed growth of the tumour throughout the host dermis and invasion of the panniculus carnosus muscle, with ulceration of the overlying skin (Figure 3C). Oral SCCs often present as an ulcerating lesion on the tongue and this was recapitulated in the orthotopic tongue xenografts (arrow, Figure 3C). There was extensive infiltration into the musculature of the tongue. Although SCC13 and SCC25 originated in different body sites, they presented similar histology in tongue and back xenografts (Figure 3C and data not shown).

Europe PMC Funders Author Manuscripts

Europe PMC Funders Author Manuscripts

Stable knockdown of FRMD4A reduces the growth rate of human SCCs and increases host survival

To evaluate the effect of FRMD4A knockdown on tumour growth we used two independent strategies, one involving a conventional shRNA approach and the other involving an inducible vector (Figure 4). We compared the effects on SCC13 and SCC25 cells growing in back skin or tongue. All cells were transduced with the luciferase/YFP construct shown in Figure 3A so that tumour growth could be measured in living mice.

We first evaluated the growth as tongue xenografts of control SCC25 (SCC25-WT), SCC25 transduced with a scrambled shRNA (SCC25-SCR) and SCC25 in which FRMD4A had been knocked down (SCC25-A7). SCC25 cells were compared with SCC13 and SJG15 (recently derived from an aggressive tongue SCC) (Figure 4A). 10^4 cells were injected into 25 mice (n=5 per cell type) and primary tumour growth was evaluated by luciferase activity at intervals. SCC13, SJG-15, SCC25-SCR and SCC25-WT grew at a similar rate and mice had to be sacrificed between days 45 and 135 because their weight had dropped by 20% or their general condition had deteriorated (Figure 4A). In contrast, growth of SCC25-A7 tumours levelled off after approximately 3 weeks and mice showed excellent long-term survival (Figure 4A). Stable knockdown of FRMD4A increased the minimum number of SCC25 cells required to form a tongue tumour from 100 to 10^4.

To evaluate the effect of FRMD4A knockdown in established tumours, SCC13 cells were infected with a Tet-on doxyxcycline inducible FRMD4A shRNA or the empty vector control (EV), and then injected into chamber grafts on the back of NSG mice. Three weeks later mice were given doxyxcycline-rich chow to induce FRMD4A knockdown. Prior to the change of diet, SCC13-EV and SCC13-FRMD4A tumours were increasing in size (Figure 4B). However, on addition of doxyxcycline SCC13-FRMD4A tumours grew significantly more slowly (Figure 4B). Survival was significantly longer in mice in which FRMD4A had been knocked down than in control mice (Figure 4B).

We also evaluated the effect of stable FRMD4A knockdown on SCC13 following injection into the tail vein of NSG mice (Figure 4C). As expected, primary tumours developed in the lungs. Mice were sacrificed after 10 days and their lungs scanned. As in the case of skin and tongue tumours, FRMD4A knockdown reduced tumour growth.

To evaluate whether FRMD4A knockdown affected metastasis as well as primary tumour growth, organs from each mouse in the experiments shown in Figure 4B were scanned in an IVIS immediately post-mortem. Lungs and liver were selected for quantification, as they are the distant organs most affected by metastases in the human disease (2). In both organs, greater levels of metastatic disease were found in mice engrafted with SCC13 expressing the empty vector control than mice in which FRMD4A was knocked down (Figure 4D). In doxycycline-treated mice injected with SCC13-EV, 5/5 had lung and 4/5 had liver metastases, whereas in mice injected with SCC13-FRMD4A 1/5 had lung and 2/5 had liver metastases.

FRMD4A knockdown reduces proliferation, stimulates differentiation and induces apoptosis of SCC cells

The xenograft experiments show that knockdown of FRMD4A decreased tumour growth and metastasis. To investigate the underlying mechanisms, histological sections of primary and secondary tumours from the experiment shown in Figure 4B were examined (Figure 5). FRMD4A knockdown tumours showed a decrease in proliferative, Ki67 positive, cells (Figure 5A) and exhibited extensive expression of the apoptosis marker cleaved caspase-3, which was not detected in control tumours (Figure 5B). This correlated with an increase in differentiation, as evaluated both by conventional histology (Figure 5A and data not shown)

Europe PMC Funders Author Manuscripts

Europe PMC Funders Author Manuscripts

and by increased expression of the terminal differentiation marker involucrin (Figure 5C). As predicted from the in vitro experiments (Figure 2), E-cadherin levels were reduced in FRMD4A knockdown tumours (Figure 5D). Labelling with SGO-3 confirmed successful knockdown of FRMD4A in tumours (Figure 5D).

We conclude that the reduced growth of tumours in which FRMD4A is knocked down reflects a reduction in proliferation, increased apoptosis and differentiation, and a decrease in levels of E-cadherin.

FRMD4A influences SCC growth by modulating the Hippo pathway

FERM domain containing proteins of the ezrin/radixin/moesin (ERM) subfamily lie downstream of receptors that mediate cell-cell and cell-extracellular matrix adhesion, including CD44, and regulate the mammalian Hippo signalling pathway (20, 21, 22, 23). Given the effects of FRMD4A on E-cadherin levels in cultured cells and tumours, we investigated whether FRMD4A regulates Hippo signalling. The primary effector of the Hippo pathway is the transcriptional co-activator YAP. Phosphorylation of YAP by LATS1/2 maintains YAP in the cytoplasm, whereas removal of LATS1/2 allows unphosphorylated YAP to enter the nucleus and associate with DNA-binding transcription factors of the TEAD/TEF family. LATS1/2 is activated through phosphorylation by a complex containing the mammalian Hippo homologues MST1 and 2 (21).

Cultured SCC13-WT, SCC13-SCR and SCC13-A7 were stained for YAP1, LATS1 and MST1 (Figure 6A and data not shown). SCC13-WT and SCC13-SCR cells showed generalised cytoplasmic staining for YAP, with minimal nuclear accumulation (Figure 6A). In contrast, on knockdown of FRMD4A YAP had a predominantly nuclear localisation (Figure 6A). FRMD4A knockdown had little effect on MST localisation, but staining of LATS was greatly reduced (Figure 6A). Western blotting revealed an overall increase in levels of YAP on FRMD4A knockdown (Figure 6B). The in vitro observations were confirmed in vivo: tumours in which FRMD4A expression was knocked down had increased nuclear YAP and reduced levels of LATS when compared with control tumours (EV) (Figure 6C and data not shown). In HNSCC the most highly differentiated tumours had the highest proportion of nuclear YAP1 (Figure 6B).

Modulating FRMD4A and the Hippo pathway to inhibit the growth of SCCs

Having established that FRMD4A levels regulate the Hippo pathway, we next investigated whether treatment of SCC cells with the CD44 ligand hyaluronan (HA) (23) had any effect on the subcellular localisation of FRMD4A. When SCC13 cells were seeded on culture dishes that had been pre-coated with HA there was a reduction in colony forming efficiency, colony area and overall growth rate (Figure 7A). This correlated with a dramatic loss of nuclear FRMD4A staining, increased CD44 labelling of apical cell surface microvilli and an increase in nuclear YAP (Figure 7B).

To test whether HA may have a potential role as a therapeutic agent in vivo, mice were xenografted with SCC13 into their back skin. Tumours were injected weekly with HA or PBS and tumour size was measured using a Xenogen IVIS. HA injected primary tumours were smaller than control tumours injected with PBS (Figure 7C) and there was also a reduction in total metastatic disease quantitated as a decrease in the combined luciferase signal from liver and lungs (Figure 7C).

Recent preclinical and clinical trials of HSP90 inhibitors have shown varying efficacy in the treatment of several cancer types and it has been suggested that they act by depletion of LATS1/2 in the Hippo pathway, thereby increasing nuclear YAP (24). Following injection of SCC13 cells into the tongue, NSG mice received weekly intraperitoneal injections of the

HSP90 inhibitor 17-DMAG (Alvespimycin) or vehicle control. 17-DMAG treated mice showed a reduction in growth of the primary tumours and decreased metastatic disease compared to controls (Figure 7C). 17-DMAG-treated tumours not only showed increased nuclear YAP but also a striking loss of nuclear FRMD4A (Figure 7D).

Discussion

We originally identified FRMD4A through gene expression profiling of single human epidermal stem cells (8) and selected it for further analysis because it was consistently upregulated in human SCC cell lines (5). By raising antibodies to the protein we have now shown that in human epidermis FRMD4A is only expressed in the basal cell layer, where the stem cells reside. In contrast, FRMD4A is upregulated in HNSCC, regardless of differentiation status, and high levels correlate with poor prognosis. Our functional studies place FRMD4A downstream of CD44 in the Hippo pathway and suggest that targeting FRMD4A is an effective treatment for skin and oral SCC.

FERM domains act as adaptors or scaffolds that interact with multiple protein partners (20). The reduction in E-cadherin-mediated adhesion that occurs on FRMD4A knockdown is consistent with the observation that FRMD4A regulates assembly of adherens junctions (9) and is also in keeping with the role of the ERM proteins in epithelial membrane organisation (20). FRMD4A differs from ERM proteins (20) in having potential nuclear localisation and nuclear export sequences (NetNES 1.1 prediction software; 25) and a leucine zipper motif (amino acids 27 to 48; 13). In support of the sequence predictions, we detected FRMD4A not only in the cytoplasm and at cell-cell borders but also in the nucleus. If, like ERM proteins, FRMD4A activity is regulated by phosphorylation-dependent interaction between the FERM domain and the C-terminus (20), unfolding could potentially reveal the NLS and leucine zipper motifs, allowing both nuclear translocation and homo- or hetero-dimerisation. CD44 ligation with HA resulted in loss of nuclear FRMD4A, indicating that transmembrane receptor signalling regulates FRMD4A localisation. In addition, FRMD4A binding to cytohesin-1 and Par-3 is required for its membrane association (9). Whether there is a direct functional interconnection between FRMD4A, CD44 and Hippo signalling, for example involving binding of FRMD4A to the CD44 cytoplasmic domain, remains to be investigated. In addition, the dependence of E-cadherin-mediated intercellular adhesion on FRMD4A suggests that FRMD4A may affect multiple signalling pathways and protein complexes.

Our in vivo studies not only indicate that targeting FRMD4A is a promising new approach for treating SCC, but also suggest possible therapeutic options, such as HSP90 drugs (24, 26) and injection of HA (27). Whereas multiple alternatively spliced forms of CD44 are expressed in SCC (23, 28), HA is consistently downregulated (29), suggesting that much of the CD44 on the surface of tumour cells is unligated. HSP90 inhibitors and HA could potentially be beneficial in HNSCC patients, either where further management by surgery or adjuvant therapies is not possible, or concurrently with standard treatment modalities.

A case can also be made for directly targeting FRMD4A, as this would potentially be more effective and specific than targeting upstream or downstream components in the signalling cascade. Two other FERM domain-containing proteins, focal adhesion kinase (FAK) and proline-rich tyrosine kinase 2 (Pyk2), have long been of interest as potential therapeutic targets in cancer (30). In the past the focus has been on inhibiting their tyrosine kinase activity, but targeting the FAK FERM domain blocks phosphorylation of the activation loop (31). There is growing evidence that targeting protein-protein interactions is achievable (32) and compounds that target the Pyk2 FERM domain have been reported (30).

Europe PMC Funders Author Manuscripts
Europe PMC Funders Author Manuscripts

Europe PMC Funders Author Manuscripts

We observed a striking reciprocal relationship between nuclear accumulation of FRMD4A and YAP, both in cultured cells and in tumours, and in those contexts increased nuclear YAP correlated with reduced growth and increased differentiation. This is unexpected, since the Hippo pathway is upregulated in many solid tumours (21), and YAP positively regulates proliferation of epidermal stem cells (33, 34). In trying to reconcile these differing observations it is worth noting that Hippo signalling is not simply a growth regulator (35). Its role as a cell density sensor may be particularly important in the context of multilayered epithelia (33). In mice, epidermal deletion of MST1/2 or LATS1/2 does not phenocopy YAP1 deletion, indicating that epidermal YAP functions independently of the canonical Hippo pathway. Instead, YAP1 forms a complex with α-catenin and 14-3-3 protein (33). Given the effect of FRMD4A knockdown on E-cadherin containing adherens junctions, it is tempting to speculate that FRMD4A may also impact on non-canonical Hippo signalling.

One final issue of interest is whether FRMD4A, a marker of normal epidermal stem cells (8), is also a cancer stem cell marker. FRMD4A is upregulated in HNSCC and knockdown stimulates terminal differentiation. It is widely expressed by cells throughout the tumour mass, and while this could potentially reflect expansion of stem cells bearing oncogenic mutations, it is surprising that it does not correlate with differentiation status. The same has been observed for another marker of normal epidermal stem cells, the β1 integrin subunit (3). Thus, rather than defining specific subsets of tumour cells, two stem cell markers, FRMD4A and β1 integrin, show a generalised upregulation in HNSCC.

Supplementary Material

Refer to Web version on PubMed Central for supplementary material.

Acknowledgments

We gratefully acknowledge the support of Hutichson Whampoa and the University of Cambridge. We also thank Kim Jensen, Julia Jones, Ellie Pryor, Rachida Nachat, Adam Giangreco and Simon Broad for their valuable input. We gratefully acknowledge the core services of the CRUK Cambridge Research Institute, Richard Price, Malcolm Cameron, Mark Thompson and Clive Moss from Addenbrooke's hospital, who made the research possible.

Financial support: MRC clinical training fellowship to SG; EU Marie Curie Fellowship to KWM (PIEF-GA-2008-220642); A* Scholarship to DWMT; core funding from Cancer Research UK (FW, SL) and Breakthrough Breast Cancer (AHS).

References

1. Patel RV, Frankel A, Goldenberg G. An update on nonmelanoma skin cancer. J Clin Aesthet Dermatol. 2011; 4:20–7. [PubMed: 21386954]
2. Argiris A, Karamouzis MV, Raben D, Ferris RL. Head and neck cancer. Lancet. 2008; 371:1695–709. [PubMed: 18486742]
3. Janes SM, Watt FM. New roles for integrins in squamous-cell carcinoma. Nat Rev Cancer. 2006; 6:175–83. [PubMed: 16498442]
4. Locke M, Heywood M, Fawell S, Mackenzie IC. Retention of intrinsic stem cell hierarchies in carcinoma-derived cell lines. Cancer Res. 2005; 65:8944–50. [PubMed: 16204067]
5. Jensen KB, Jones J, Watt FM. A stem cell gene expression profile of human squamous cell carcinomas. Cancer Lett. 2008; 272:23–31. [PubMed: 18657901]
6. Prince ME, Sivanandan R, Kaczorowski A, Wolf GT, Kaplan MJ, Dalerba P, et al. Identification of a subpopulation of cells with cancer stem cell properties in head and neck squamous cell carcinoma. Proc Natl Acad Sci USA. 2007; 104:973–8. [PubMed: 17210912]
7. Gupta PB, Chaffer CL, Weinberg RA. Cancer stem cells: mirage or reality? Nat Med. 2009; 15:1010–2. 2009. [PubMed: 19734877]

Europe PMC Funders Author Manuscripts

8. Jensen KB, Watt FM. Single-cell expression profiling of human epidermal stem and transit-amplifying cells: Lrig1 is a regulator of stem cell quiescence. Proc Natl Acad Sci USA. 2006; 103:11958–63. [PubMed: 16877544]
9. Ikenouchi J, Umeda M. FRMD4A regulates epithelial polarity by connecting Arf6 activation with the PAR complex. Proc Natl Acad Sci USA. 2010; 107:748–53. [PubMed: 20080746]
10. Cohen J, Chen Z, Lu SL, Yang XP, Arun P, Ehsanian R, et al. Attenuated transforming growth factor beta signaling promotes nuclear factor-kappaB activation in head and neck cancer. Cancer Res. 2009; 69:3415–24. [PubMed: 19351843]
11. Chung CH, Parker JS, Karaca G, Wu J, Funkhouser WK, Moore D, et al. Molecular classification of head and neck squamous cell carcinomas using patterns of gene expression. Cancer Cell. 2004; 5:489–500. [PubMed: 15144956]
12. Camp RL, Dolled-Filhart M, Rimm DL. X-tile: a new bio-informatics tool for biomarker assessment and outcome-based cut-point optimization. Clin Cancer Res. 2004; 10:7252–9. [PubMed: 15534099]
13. Rheinwald JG, Beckett MA. Tumorigenic keratinocyte lines requiring anchorage and fibroblast support cultures from human squamous cell carcinomas. Cancer Res. 1981; 41:1657–63. [PubMed: 7214336]
14. Miyoshi H, Blomer U, Takahashi M, Gage FH, Verma IM. Development of a self-inactivating lentivirus vector. J Virol. 1998; 72:8150–7. [PubMed: 9733856]
15. Zufferey R, Dull T, Mandel RJ, Bukovsky A, Quiroz D, Naldini L, et al. Self-inactivating lentivirus vector for safe and efficient in vivo gene delivery. J Virol. 1998; 72:9873–80. [PubMed: 9811723]
16. Arwert EN, Lal R, Quist S, Rosewell I, van Rooijen N, Watt FM. Tumor formation initiated by nondividing epidermal cells via an inflammatory infiltrate. Proc Natl Acad Sci USA. 2010; 107:19903–8. [PubMed: 21041641]
17. Poulsom R, Longcroft JM, Jeffery RE, Rogers LA, Steel JH. A robust method for isotopic riboprobe in situ hybridisation to localise mRNAs in routine pathology specimens. Eur J Histochem. 1998; 42:121–32. [PubMed: 9728289]
18. Jensen KB, Driskell RR, Watt FM. Assaying proliferation and differentiation capacity of stem cells using disaggregated adult mouse epidermis. Nat Protoc. 2010; 5:898–911. [PubMed: 20431535]
19. http://myhits.isb-sib.ch
20. Fehon RG, McClatchey AI, Bretscher A. Organizing the cell cortex: the role of ERM proteins. Nat Rev Mol Cell Biol. 2010; 11:276–87. [PubMed: 20308985]
21. Pan D. The hippo signalling pathway in development and cancer. Dev Cell. 2010; 19:491–505. [PubMed: 20951342]
22. Xu Y, Stamenkovic I, Yu Q. CD44 attenuates activation of the hippo signalling pathway and is a prime therapeutic target for glioblastoma. Cancer Res. 2010; 70:2455–64. [PubMed: 20197461]
23. Zöller M. CD44: can a cancer-initiating cell profit from an abundantly expressed molecule? Nat Rev Cancer. 2011; 11:254–67. [PubMed: 21390059]
24. Huntoon CJ, Nye MD, Geng L, Peterson KL, Flatten KS, Haluska P, et al. Heat shock protein 90 inhibition depletes LATS1 and LATS2, two regulators of the mammalian hippo tumor suppressor pathway. Cancer Res. 2010; 70:8642–50. [PubMed: 20841485]
25. http://www.cbs.dtu.dk
26. Holzbeierlein JM, Windsperger A, Vielhauer G. Hsp90: a drug target? Curr Oncol Rep. 2010; 12:95–101. [PubMed: 20425593]
27. Gibbs P, Clingan PR, Ganju V, Strickland AH, Wong SS, Tebbutt NC, et al. Hyaluronan-Irinotecan improves progression-free survival in 5-fluorouracil refractory patients with metastatic colorectal cancer: a randomized phase II trial. Cancer Chemother Pharmacol. 2011; 67:153–63. 2011. [PubMed: 20333384]
28. Hudson DL, Speight PM, Watt FM. Altered expression of CD44 isoforms in squamous-cell carcinomas and cell lines derived from them. Int J Cancer. 1996; 66:457–63. [PubMed: 8635860]
29. Sironen RK, Tammi M, Tammi R, Auvinen PK, Anttila M, Kosma VM. Hyaluronan in human malignancies. Exp Cell Res. 2011; 317:383–91. [PubMed: 21134368]

Europe PMC Funders Author Manuscripts

30. Meurice N, Wang L, Lipinski CA, Yang Z, Hulme C, Loftus JC. Structural conservation in band 4.1, ezrin, radixin, moesin (FERM) domains as a guide to identify inhibitors of the proline-rich tyrosine kinase 2. J Med Chem. 2010; 53:669–77. 2010. [PubMed: 20017492]
31. Lietha D, Cai X, Ceccarelli DF, Li Y, Schaller MD, Eck MJ. Structural basis for the autoinhibition of focal adhesion kinase. Cell. 2007; 129:1177–87. [PubMed: 17574028]
32. Wells JA, McClendon CL. Reaching for high-hanging fruit in drug discovery at protein-protein interfaces. Nature. 2007; 450:1001–9. [PubMed: 18075579]
33. Schlegelmilch K, Mohseni M, Kirak O, Pruszak J, Rodriguez JR, Zhou D, et al. Yap1 acts downstream of α-catenin to control epidermal proliferation. Cell. 2011; 144:782–95. [PubMed: 21376238]
34. Zhang H, Pasolli HA, Fuchs E. Yes-associated protein (YAP) transcriptional coactivator functions in balancing growth and differentiation in skin. Proc Natl Acad Sci USA. 2011; 108:2270–5. [PubMed: 21262812]
35. Halder G, Johnson RL. Hippo signalling: growth control and beyond. Development. 2011; 138:9–22. [PubMed: 21138973]

Europe PMC Funders Author Manuscripts

Europe PMC Funders Author Manuscripts

Europe PMC Funders Author Manuscripts

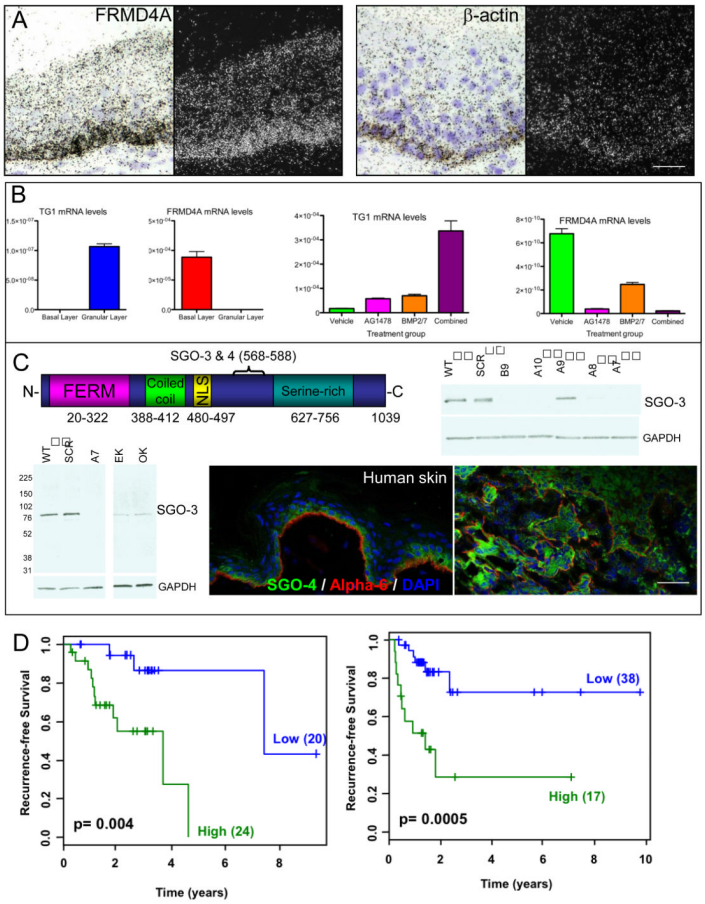

Figure 1. FRMD4A is expressed in basal cells of human epidermis and upregulated in HNSCC

(A) In situ hybridisation of FRMD4A and β-actin in neonatal human foreskin. Dark and bright field images of the same sections are shown. (B) Q-PCR of transglutaminase1 and FRMD4A mRNA levels (relative to 18S mRNA) in different layers of adult human epidermis obtained by laser capture microdissection (left hand panels) and in cultured human keratinocytes treated with the differentiation inducing agents shown (right hand panels). Data are means ± SEM of 3 technical replicates (laser capture) or triplicate samples (cultured cells). (C) Detection of FRMD4A protein. Predicted domain structure of FRMD4A protein and location of SGO-3, 4 antibody epitopes. Western blots were probed for FRMD4A (SGO-3) or GAPDH (loading control). WT: control SCC13; SCR: SCC13 transduced with scrambled control shRNA; B9, A7, A8, A9, A10: independent shRNAs to FRMD4A; EK: epidermal keratinocytes; OK: oral keratinocytes. Molecular mass markers (kDa) are indicated. Sections of human abdominal skin and human tongue squamous cell carcinoma were labelled with antibodies to FRMD4A (green; SGO-4) and α6 integrin (red) with DAPI nuclear counterstain. Scale bars: 50μm. (D) Kaplan Meier plots from two independent datasets (LHS: ref 10; RHS: ref 11). Blue indicates low and green represents high FRMD4A expression. The number of tumours in each group is given in brackets. The optimum cut-point was determined using the method of Camp et al. (12).

Europe PMC Funders Author Manuscripts

Europe PMC Funders Author Manuscripts

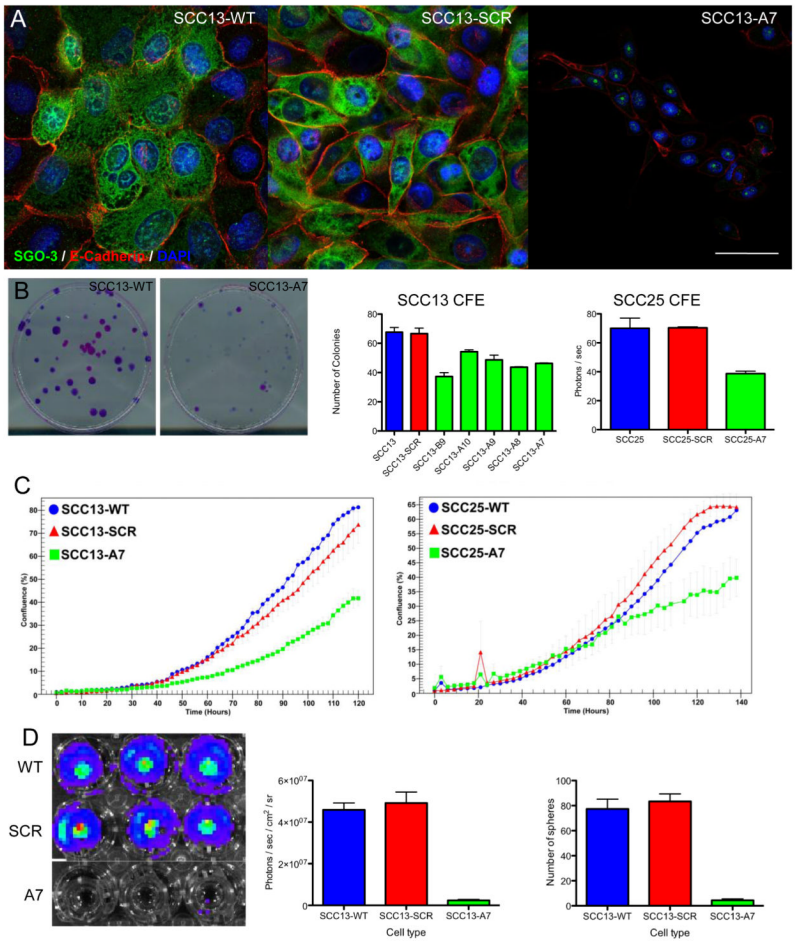

Figure 2. Effect of FRMD4A knockdown on human SCC cells in culture

Control cells (WT) were compared with cells transduced with scrambled shRNA (scr) and FRMD4A shRNAs. (A) SCC13 cells labelled with anti-FRMD4A (green) and E-cadherin (red) with DAPI nuclear counterstain (blue). Residual nuclear staining for FRMD4A following knockdown is non-specific. Scale bars: 20μm. (B) Clonal growth of SCC13 and SCC25 cells. Representative dishes stained with Rhodanile B to reveal individual clones are shown. Data are means ± SEM of triplicate dishes. FRMD4A significantly inhibited colony forming efficiency ($P < 0.01$). (C) Growth curves of SCC13 and SCC25. (D) SCC13 Matrigel invasion and sphere formation. Luciferase activity in representative wells of the invasion assay are shown (left hand panel) and quantitated (middle panel). Right hand panel shows % cells that formed spheres in suspension. Data are means ± SEM of triplicate dishes. FRMD4A knockdown significantly reduced Matrigel invasion and sphere formation ($P < 0.001$).

Europe PMC Funders Author Manuscripts

Europe PMC Funders Author Manuscripts

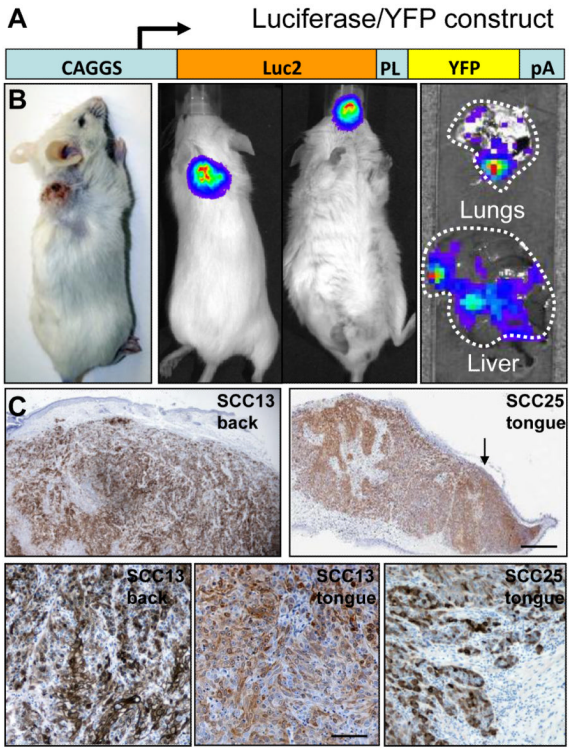

Figure 3. Primary tumours and metastases formed by orthotopic xenografts in NSG mice

(A) Luciferase/YFP lentiviral vector used to transduce cells. PL: 26 amino acid peptide linker; pA: polyadenylation sequence. (B) Macroscopic appearance of tumours. SCC13 tumour on back (left hand panel). Luciferase activity in primary SCC13 tumour on back (second from left) and SCC25 tumour in oral cavity (second from right) and in metastases to lungs and liver (right hand panels). (C) Primary tumours labelled with anti-GFP, which cross-reacts with YFP (brown) and haematoxylin. SCC13 and SCC25 tumours in back skin and tongue are shown. Scale bars: 250μm (upper panels), 50μm (lower panels).

Europe PMC Funders Author Manuscripts

Europe PMC Funders Author Manuscripts

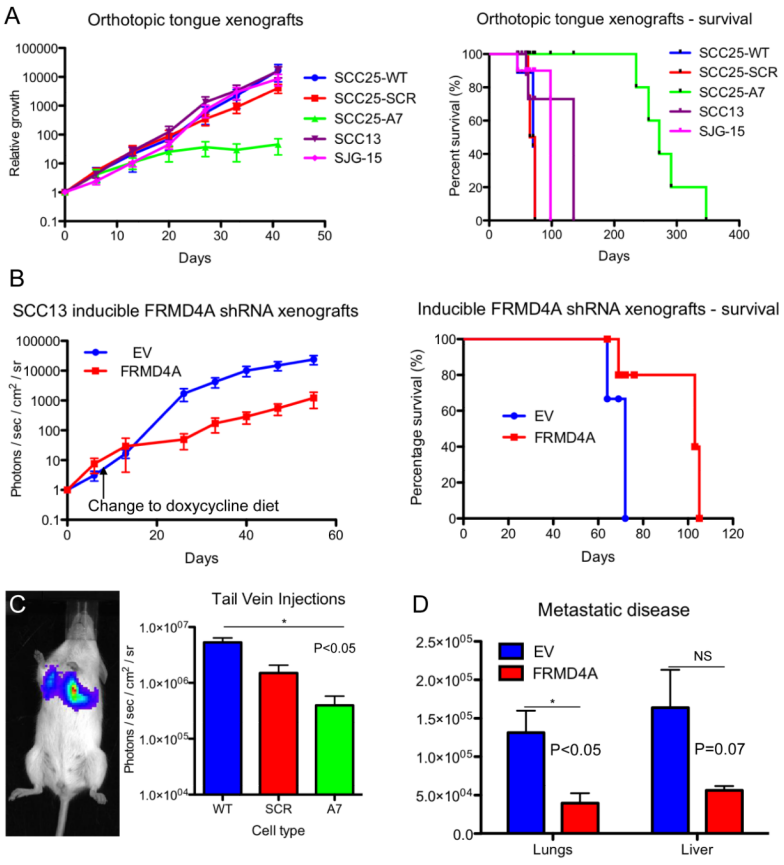

Figure 4. Knockdown of FRMD4A reduces growth and metastasis of SCC in vivo

(A) Tumour growth and survival rates of mice with tongue xenografts. (B) Tumour growth and survival rates of SCC13 dorsal skin xenografts. Left hand panel: Day 0 is first scan (14 days after grafting). Mice were switched to diet of mash containing doxycycline on day 8 after first scan. Right hand panel: Day 0 is day of grafting. (C) Lung tumours formed 10 days after tail vein injection of SCC13. Quantitation of luciferase activity is shown. (D) Quantitation of metastatic disease in lungs and livers of mice xenografted with inducible SCC13. Luciferase measurements were made of isolated organs at end-point of experiments shown in (B). Data are means ± SEM of triplicate mice. *P < 0.05. (A, C) Control cells (WT) were compared with cells transduced with scrambled shRNA (SCR) and FRMD4A shRNA (A7). (B, D). Control cells transduced with empty lentiviral vector (EV) were compared with cells with doxycyline-inducible FRMD4A knockdown (FRMD4A).

Europe PMC Funders Author Manuscripts

Europe PMC Funders Author Manuscripts

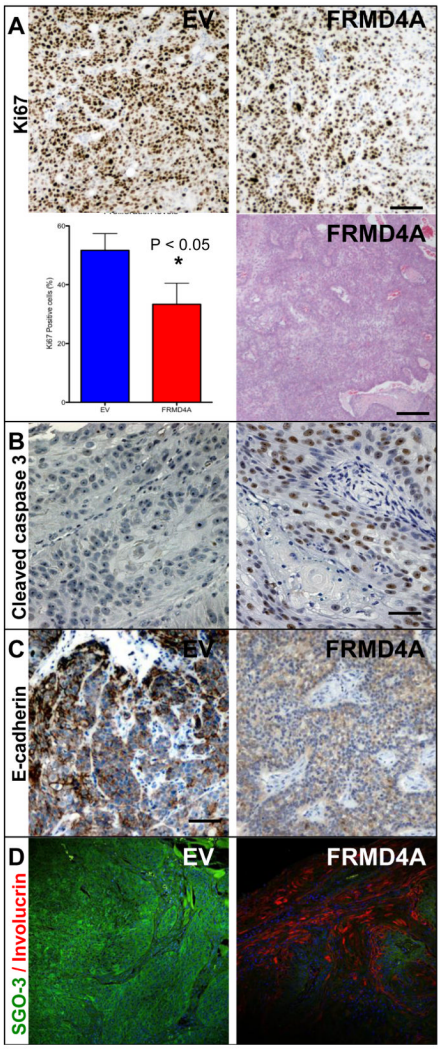

Figure 5. Knockdown of FRMD4A reduces proliferation, induces apoptosis and stimulates differentiation of SCC13 back skin xenografts

Cells were either transduced with FRMD4A shRNA (FRMD4A) or empty vector control (EV). (A) Ki67 labelling and tumour histology. Data are means ± SEM of single sections from three independent tumours. *P < 0.05. Haematoxylin and eosin staining shows areas of keratinisation (pink), indicating that tumour is well differentiated. (B) Cleaved caspase-3 (brown) with haematoxylin counterstain. (C) E-cadherin labelling (brown) with haematoxylin counterstain. (D) FRMD4A (green) and involucrin (red) labelling with DAPI nuclear counterstain (blue). Scale bars: 50μm (H&E staining in A), 20μm (all other panels).

Europe PMC Funders Author Manuscripts

Europe PMC Funders Author Manuscripts

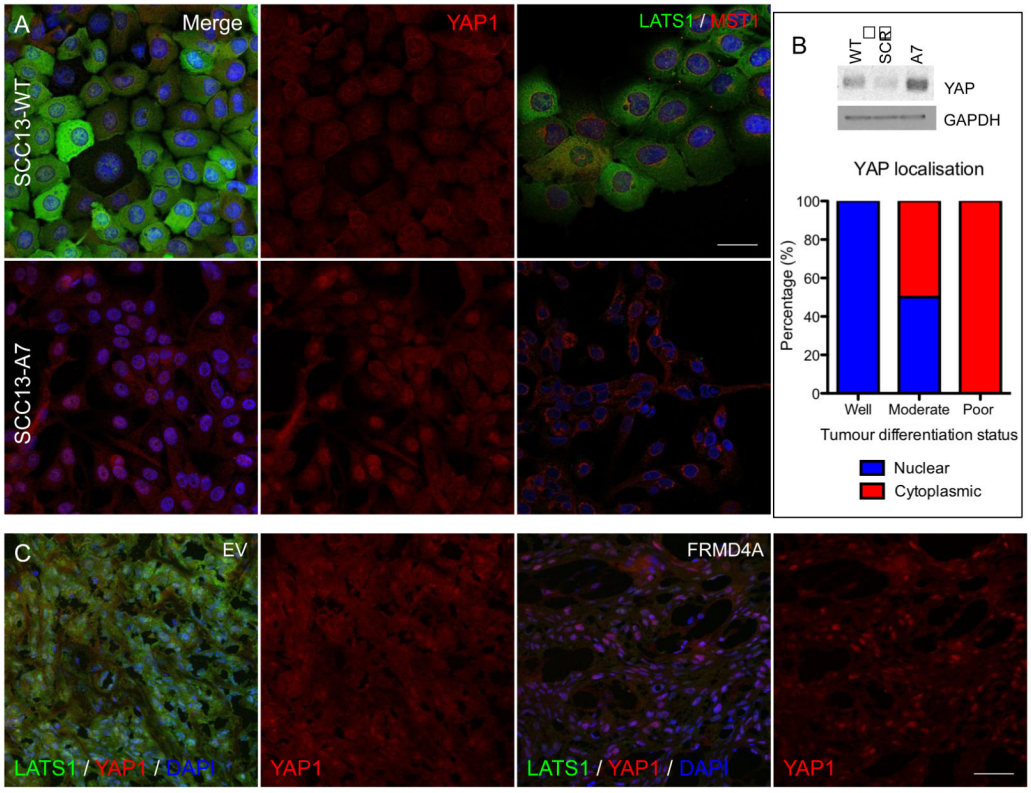

Figure 6. FRMD4A regulates the HIPPO pathway

(A) Untransduced (WT), FRMD4A shRNA (A7) or scrambled shRNA (SCR) transduced SCC13 cells were labelled with antibodies to FRMD4A (green, left hand panels) and YAP1 (red, middle panels) or LATS1 (green, right hand panels) and MST1 (red, right hand panels) and counterstained with DAPI (blue). Left hand and middle panels are each show same field. (B) Western blot probed for YAP1 and GAPDH (loading control) and quantitation of average % cells with nuclear or cytoplasmic YAP1 in human oral SCCs of differing differentiation status (n=4 for each tumour type). (C) SCC13 back skin xenografts labelled for LATS1 (green) and YAP1 (red) with DAPI nuclear counterstain (blue). Cells were transduced with empty lentiviral vector (EV) or doxycycline-inducible FRMD4A shRNA. Scale bars: 10μm (A), 20μm (C).

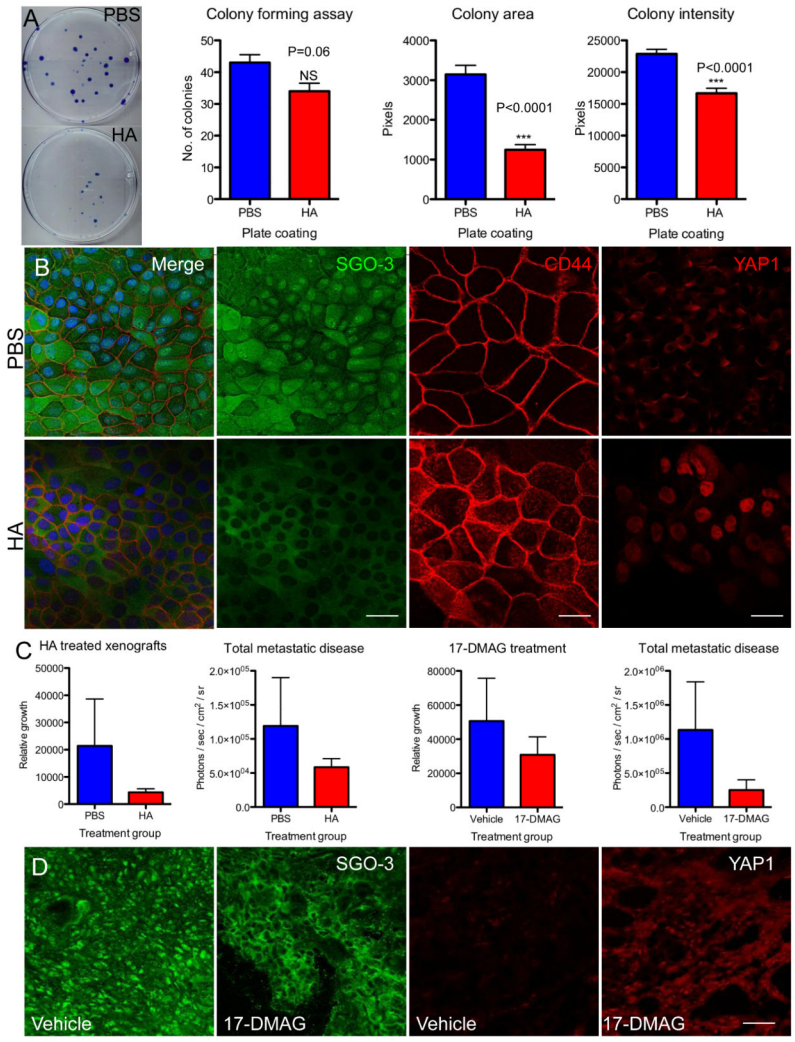

Figure 7. Modulating FRMD4A and HIPPO via HA or 17-DMAG reduces SCC growth in vitro and in xenografts

(A) SCC13 cells grown at clonal density on culture dishes coated with PBS or HA. Representative dishes stained with rhodanile blue are shown. % colony formation, colony area and colony staining intensity (readout of cell density per unit colony area) were quantitated Data are means ± SEM of triplicate dishes. (B) SCC13 cells grown on coverslips coated with PBS or HA and labelled with antibodies to FRMD4A (green) and CD44 (red), or YAP1 (red). Left hand and second from left panels are pairs of images showing same fields. (C) Effect of HA or 17-DMAG treatment on primary tumour growth (SCC13 in the case of HA; SCC25 in the case of 17-DMAG) and total metastatic disease (combined values for liver and lungs) in tongue xenografts. Quantitative data are means ± SEM (n=5). (D) Sections of primary tumours were labelled with antibodies to FRMD4A (green) or YAP1 (red). Scale bars: 10μm (B), 20μm (D).

Europe PMC Funders Author Manuscripts
Europe PMC Funders Author Manuscripts